LIMNOLOGY and OCEANOGRAPHY

Weak mineralization despite strong processing of dissolved organic matter in Eastern Arctic tundra ponds

Isabelle Laurion [ORCID],[1]* Philippe Massicotte,[2] Flora Mazoyer,[1] Karita Negandhi,[1,3] Natalie Mladenov[4]

[1]Centre for Northern Studies and Centre Eau Terre Environnement, Institut National de la Recherche Scientifique, Quebec City, Quebec, Canada
[2]Takuvik and Laval University, Quebec City, Quebec, Canada
[3]Department of Planning, Infrastructure and Environment, New South Wale Government, Parramatta, New South Wales, Australia
[4]Department of Civil, Construction, and Environmental Engineering, San Diego State University, San Diego, California

Abstract

Permafrost thawing mobilizes large quantities of organic carbon that was sequestered in Arctic regions over the last glacial cycle. Processes involved in the oxidation of this carbon need to be further assessed to estimate the fraction to be released into the atmosphere. Shallow tundra ponds are sites of active carbon turnover on the landscape and significant sources of greenhouse gases. Dissolved organic matter (DOM) leached from thawing peat into these ponds is exposed to sunlight, with the potential to accelerate its mineralization directly into CO_2 or through the production of more labile molecules. We tested the catalytic effect of sunlight on DOM mineralization in tundra ponds formed on organic-rich polygonal landscapes originating from syngenetic permafrost, including a pond exposed to active permafrost erosion. Microbial decay rates, measured as the loss of chromophoric DOM, were similar to photodecay rates (1%–3% d^{-1}). Groups of fluorescing molecules were formed through microbial transformation or lost through photolysis at differing rates among studied ponds, with the erosive trough pond presenting a unique response suggesting the involvement of soil microbes. Despite the stimulation of microbial growth under sunlight and the dynamic response of DOM optical properties, the loss of dissolved organic carbon was not significant under any treatment. This suggests that microbial and photochemical mineralization of DOM was slow and potentially substrate-limited during the dry period when ponds were sampled. The static nature of tundra ponds, with their long water retention time, may thus constrain hot moments when water moves and transports carbon on the landscape.

Seasonal thawing of surficial permafrost is associated with waterlogging on many tundra landscapes (Grosse et al. 2013). The accelerated warming of the Arctic intensifies soil erosion and subsidence in ice-rich areas and the transfer of terrestrial carbon (C) and nitrogen to aquatic systems (Schuur et al. 2015; Vonk et al. 2015; Wauthy et al. 2018). In addition, climate warming lengthens the ice-free season (Surdu et al. 2016), which further contributes to the warming of surface waters

(O'Reilly et al. 2015) and the increased exposure of water bodies to solar radiation (Williamson et al. 2014). The vast organic C pool locked in permafrost-affected soils (estimated at ~ 1300 Pg, Hugelius et al. 2014) is now partly mobilized to the hydrosphere in the form of dissolved organic matter (DOM) as permafrost thaws. The combination of warming and longer periods of solar exposure has the potential to accelerate the mineralization of this C. There is not yet a consensus on the importance of ancient C mineralization in disrupting the global C cycle (Gao et al. 2013; Drake et al. 2015; Comyn-Platt et al. 2018; Elder et al. 2018; Knoblauch et al. 2018; Bogard et al. 2019). However, recent estimations suggest that thawing could release to aquatic systems ~ 15% of the soil C currently stored in permafrost regions over the next 300 yr under a business-as-usual warming scenario (McGuire et al. 2018). The fate of this C pool needs to be evaluated since even a partial transfer to the atmosphere could result in a positive feedback onto climate warming (Turetsky et al. 2020). Tundra lakes and ponds may be a critical element of this transfer where

conditions favor C mineralization, particularly as they are increasing in importance in many regions of the Arctic (Lara et al. 2015; Liljedahl et al. 2016; Martin et al. 2017).

In surface waters, DOM is concurrently exposed to photochemical and biological degradation (Obernosterer and Benner 2004), two processes that contribute to the release of greenhouse gases (GHG) into the atmosphere. The relative contribution of these processes to the overall C budget of a lake depends on sunlight availability, water residence time, mixing regime, and the intrinsic properties of DOM (Lapierre and del Giorgio 2014; Cory and Kling 2018). As shown through quantum yield determinations (Groeneveld et al. 2016 and references therein), ultraviolet radiation (UVR) is most efficient at transforming and mineralizing DOM, but is quickly attenuated in the water column of colored lakes. While only surface waters are exposed to significant radiation, depending on the mixing regime, this layer can be renewed on a daily cycle (Forrest et al. 2008), increasing the efficiency of C cycling through photobleaching.

Many studies have underscored how sunlight can efficiently degrade DOM since the 1970s (Strome and Miller 1978), although this effect is not always measured in C cycle investigations. Photochemical oxidation of DOM is considered an important removal mechanism of terrestrial DOM in Arctic freshwaters (Cory et al. 2014). It occurs through two pathways: direct abiotic production of CO_2 through complete photooxidation of DOM, and indirect production of CO_2 through microbial respiration of smaller and more bioavailable photoproducts (Vähätalo et al. 2003; Cory and Kling 2018). To explore the synergistic effects of biotic and abiotic pathways, microbial and photochemical DOM decay need to be assessed concurrently.

Microbial respiration of allochthonous DOM is considered as the main driver of lake CO_2 supersaturation. However, because chemical and optical characteristics of DOM and the underwater light field are complex and variable across landscapes, the contribution of photodegradation to freshwater CO_2 production is not well constrained. According to a global upscaling exercise for lakes and reservoirs worldwide, but based on results obtained on Swedish lakes, only about one-tenth of freshwater CO_2 emissions would originate from direct photomineralization (Koehler et al. 2014). On the other hand, the importance of photomineralization was shown to vary seasonally, reaching 49% of the total pelagic CO_2 production after ice melt for a boreal lake (Vachon et al. 2016). With ongoing climate change affecting many physical features of lakes including ice-cover duration, water residence time and mixing regimes, the accelerated decay of DOM caused by sunlight appears as a fundamental factor to consider in C cycling assessments (Wrona et al. 2016).

The few studies addressing DOM degradation in permafrost regions present fairly contrasting results. For example, ancient DOM from Yedoma permafrost thaw streams was shown to be highly biolabile (Vonk et al. 2013; Abbott et al. 2014; Drake et al. 2015; Mann et al. 2015). Moreover, studies of waters of the North Slope of Alaska near Toolik (syngenetic permafrost with variable organic and ice contents) indicated that DOM was highly susceptible both to direct and indirect photomineralization (Cory et al. 2013), with photooxidation suggested as the dominant oxidation process in Arctic freshwaters (Cory et al. 2014). On the other hand, no CO_2 was produced directly out of photodegradation, at least in the Kolyma River basin (Stubbins et al. 2017). Furthermore, incubations of High Arctic pond DOM to sunlight also revealed the absence of significant loss in dissolved organic carbon (DOC) over a few days, but a rapid loss of color and the cleavage of large molecules into smaller moieties (Laurion and Mladenov 2013). Humic waters from frozen peat bogs in Siberia were shown to be resistant to both photochemical and microbial mineralization (Shirokova et al. 2019), and low biolability of permafrost soil organic matter has been recently reported (Kuhry et al. 2020). Much still remains to be understood regarding the combined effects of microbial and sunlight degradation processes on DOM mineralization in Arctic freshwaters.

The overarching objective of this study was to assess if pelagic DOM processing contributes to CO_2 production in Canadian Arctic ponds with variable origins (topographic and thermokarstic). Ponds are an abundant component of the polygonal tundra landscapes and large GHG emitters in summer (Bouchard et al. 2015). They receive inputs of organic matter from surrounding peaty soils as well as from benthic and littoral primary producers thriving in these shallow systems, which are exposed to sunlight for about 3 months per year. Using field experiments to concurrently quantify the biodegradation and photodegradation of DOM under natural conditions, we tested the hypothesis that sunlight accelerates DOM mineralization in tundra ponds of a non-Yedoma region, particularly in trough ponds that are impacted by permafrost subsidence and erosion. This study contributes to the understanding of Arctic DOM degradability, focusing on an overlooked geographical area.

Methods

Study site and selected ponds

The studied ponds are located in a glacier valley of Sirmilik National Park on Bylot Island, Nunavut, Canada (73°N, 80°W), in a region of continuous syngenetic permafrost cryoturbated by the formation and decay of ice wedges. Although this site is not located within regions where the largest C stocks were identified for the frozen north (Hugelius et al. 2014), the studied valley represents many other circumpolar, polygonal landscapes that contain vast stocks of C, including the Lena Delta (Abnizova et al. 2012) and the Barrow Peninsula (Lara et al. 2015). Soils are composed of alternating peat and wind-blown sand and silt materials, which started to accumulate over glaciofluvial sands and gravels around 3700 years ago (Fortier and Allard 2004). These

deposits contain excess pore ice, and their gravimetric organic matter content can reach over 50%, with an active layer depth generally ranging between 40 and 60 cm (D. Fortier, pers. comm.). Sedges, grasses, brown mosses, and cyanobacterial mats dominate primary production in this area.

We selected four ponds to cover the range of morphological and limnological conditions found on this type of landscape (Table 1). Two ponds classified as *polygonal ponds* (BYL1 and BYL22) are lying over low-center polygons. BYL1 is a coalescent polygonal pond formed by pond expansion through thermoerosion and wave action, connecting several polygonal and trough ponds into one system, while BYL22 is a water body in the depression of one low-center peat polygon, with a much smaller volume, and which has already progressed to merge two polygons since 2010. The two others, classified as *trough ponds* (BYL24 and BYL38), are elongated water channels formed in collapsed ice-wedge troughs. Trough pond BYL38 is located on the side of a hill and highly influenced by thermoerosional processes of melting snowbanks and has quickly evolved and enlarged since 2010, while BYL24 (also influenced by thermoerosion but with a smaller drainage area) is relatively stabilized and colonized by graminoids and brown mosses. Because of these differences, the four ponds selected are characterized by DOM of differing optical properties even though they are close to each other (Table 1). Since the ponds are not connected via a hydrologic network, it is assumed that pond DOM takes its source from the immediate vicinity, including from living terrestrial and aquatic plants, and organic matter of the active layer and eroding permafrost. Although the proportion of these sources has not been determined in the studied ponds, Fortier and Allard (2004) have shown for this specific site the upward displacement of deeper (older) sedimentary strata along the ice wedges, which then get exposed to surface thawing. Field observations also indicate active erosion on the shores of pond BYL38. Therefore, we assume eroding trough ponds have a higher potential to receive older C on this landscape.

Environmental and limnological conditions

Incident photosynthetically available radiation (PAR) at the water surface and air temperature were recorded by a nearby meteorological station (CEN 2018) during the experiments (all ponds located within 1 km distance of the station). The incident spectrum for a typical sunny day at this latitude and dates was also obtained from Sequoia Scientific Inc. (Hydrolight software). A chain of temperature loggers (Onset

Table 1. Morphological and limnological properties of the four studied ponds in 2010 (surface water initial conditions), including pond area, maximal depth, total phosphorus (TP), soluble reactive phosphorus (SRP), total nitrogen (TN), nitrate (NO_3), chlorophyll *a* as an index of planktonic biomass (Chl *a*), total suspended solids (TSS), total dissolved iron (Fe), dissolved organic carbon (DOC), DOM absorption coefficient at 320 nm (a_{320}), absorption slope at 285 nm (S_{285}), SUVA index, and biological index of fluorescent DOM (BIX). Median values for near-by polygonal and trough ponds sampled in 2009 are added for comparison.

Pond name	BYL1	BYL22	BYL24	BYL38	Median Polygonal $n = 11$	Median Trough $n = 20$
Pond type	Coalescent polygonal	Low-centered polygonal	Stabilized trough	Eroding trough		
Max depth* (m)	0.8	0.2	1.0	0.8	na	na
Area (m^2)	428	33	88	99	na	na
Volume (m^3)	165[†]	14[†]	38	40[†]	na	na
TP (μg P L^{-1})	18.6	68.1	38.0	54.2	17.1	31.9
SRP (μg P L^{-1})	0.5	0.5	1.6	4.7	0.3	0.7
TN (mg N L^{-1})	0.51	0.36	0.41	0.51	0.4	0.9
NO_3 (mg N L^{-1})	0.07	0.09	0.12	0.10	0.06	0.07
Chla (μg L^{-1})	0.6	1.9	1.0	1.1	1.3	1.2
TSS (mg L^{-1})	1.3	5.3	5.8	8.0	na	na
Fe (mg L^{-1})	0.45	0.86	1.32	3.05	0.4	1.0
DOC (mg L^{-1})	8.9	9.9	7.9	11.2	9.2	12.5
a_{320} (m^{-1})	13.2	20.8	36.3	67.3	15.4	39.4
S_{285} (nm^{-1})	0.0188	0.0143	0.0125	0.0114	0.0201	0.0154
SUVA[‡] (L mg DOC^{-1} m^{-1})	1.8 (1.5)	2.1 (1.5)	4.3 (3.2)	5.4 (3.6)	2.1	3.3
BIX	0.70	0.61	0.46	0.46	0.62	0.52
Date sampled	10 July	11 July	11 July	12 July	—	—

na, not available.

*Depth may have changed during the summer according to meteorological conditions but was measured only once.

[†]Volume estimated from the area and average pond depth, while the precise bathymetry was available for BYL24.

[‡]Values in parentheses correspond to SUVA values corrected after Poulin et al. (2014) for Fe concentration.

Table 2. Description of the incubation treatments.

Color code	Treatment code	Filtration step	Sunlight exposure
(green)	C	0.2 μm	No
(blue)	B	No	No
(yellow)	S	0.2 μm	Yes
(red)	BS	No	Yes

StowAway TidbiT; accuracy 0.4°C, resolution 0.3°C) was installed in BYL1 and BYL38 at 0, 10, 20, 40, 60 and 80 cm depth to follow the thermal structure along the experiments, in addition to loggers placed in the incubation setting (one pair of loggers per pond in dark and light treatments for BYL1 and BYL38). Basic limnological properties of the ponds, including pond morphology, nutrients, phytoplanktonic biomass, suspended solids, and iron concentration, were measured as described in Laurion et al. (2010) and Negandhi et al. (2014).

Water incubation

The effect of sunlight and microbes on DOM degradation was tested using a three-way factorial design. The microbial assemblage responsible for DOM degradation could include Archaea and small protozoans, although the settings used for cell counts by flow cytometry likely only included the population of bacteria. Therefore, the term "bacteria" is used below for simplicity. The contrasting optical properties of the four ponds were used to test the effect of intrinsic DOM properties on degradation rates concomitant with effects by differing spectral exposure, as water from each pond was incubated under its respective environmental conditions. The water was collected on 10 July (BYL1), 11 July (BYL24 and BYL38), and 12 July 2010 (BYL22). The in situ incubations lasted 12 d, with subsampling on Days 4, 7, and 12 (the exact sampling time varied among ponds).

Four treatments were applied: (1) *Control* (C) obtained by filtering water through 0.2 μm (prerinsed cellulose acetate filters, Advantec Microfiltration Systems) incubated in the dark; (2) *Bacteria* (B) obtained on unfiltered water incubated in the dark; (3) *Sunlight* (S) obtained using the same filtered water but incubated under natural sunlight conditions; (4) *Sunlight and Bacteria* (SB) obtained on unfiltered water incubated under natural light conditions (Table 2). In the SB treatment, DOM microbial degradation was not consecutive to sunlight exposure but rather represents the concomitant biodegradation and photodegradation in the presence of potentially deleterious UVR.

Water was incubated in 60-mL Teflon (sunlight) or glass (dark) bottles. Teflon bottles are known for their transparency to UVR despite the diffusive property of this material. A total of 36 bottles were incubated in each pond, allowing the collection of three replicate bottles per treatment per sampling day. Dark was achieved using black bags covered with reflective tape and filled with ambient water to minimize temperature differences among treatments. The temperature loggers were deployed besides sunlight and dark treatment bottles of BYL1 and BYL38 to measure any discrepancies in water temperature. Bottles were floating at about 5 cm below the water surface (see Laurion and Mladenov 2013 for light exposure calculations at this depth for a typical summer day at this latitude). At each sampling day, the three replicate bottles were brought back to the camp where samples were treated to measure the bacterial abundance and DOM properties.

DOM properties

For DOM characterization, water was filtered (or refiltered in the case of Control and Sunlight treatments) using a syringe and capsule filter (prerinsed 0.2 μm cellulose acetate) and stored in 40-mL glass bottles in the dark at 4°C until spectrally analyzed back in the laboratory (within 4 weeks after the end of the experiment). The chromophoric and fluorescent fractions of DOM (CDOM, FDOM) and the DOC were analyzed from the same bottle. After optical analyses were performed, the remaining water was acidified for DOC analyses. Therefore, any changes potentially occurring in the DOM composition between the end of experiment and the completion of analyses would be consistent among results. DOC concentrations were measured using a Shimadzu TOC-VCPH carbon analyzer calibrated with potassium biphthalate standards. To characterize CDOM, absorbance scans were performed between 200 and 800 nm on a dual-beam spectrophotometer (Varian Cary 300) at a speed of 240 nm min^{-1} and a slit width of 2 nm. Spectroscopic measurements were always run at natural pH and at room temperature using 1-cm path length quartz cuvettes. Spectra were null-point adjusted (the average absorbance between 790 and 800 nm was subtracted from the whole spectrum). The absorption coefficient at 320 nm ($a_{CDOM}(320)$, shortened to a_{320}) was used as a quantitative proxy of CDOM. The spectral slope curves S_λ were obtained according to Loiselle et al. (2009) with a wavelength interval size of 20 nm. The slope at 285 nm (S_{285}; calculated from 275 to 295 nm) was selected as a responsive qualitative proxy on CDOM. The specific ultraviolet absorbance (SUVA) index (absorbance at 254 nm per unit DOC) was also calculated. The SUVA index corrected for Fe concentration according to Poulin et al. (2014) is presented in Table 1 (in parentheses).

Fluorescence properties of DOM (FDOM) were further characterized by excitation–emission matrices (EEMs) and the components extracted with PARAFAC (Murphy et al. 2013). EEM fluorescence was innerfilter-corrected, blank-subtracted, and Raman-normalized. A five-component model (C1–C5) was validated on the present data set that also included a series of EEMs originating from 33 aquatic systems located at the same site (including one creek, one kettle lake, one thermokarst lake, 20 trough ponds and 11 polygonal ponds,

1 some sampled a few times over 2 years), to further increase
2 the sensitivity of the model. PARAFAC modeling was per-
3 formed according to Stedmon and Bro (2008) using the
4 Matlab drEEM toolbox (Murphy et al. 2013). Before modeling,
5 Rayleigh scatter bands were excised (first order at each wave-
6 length pair where excitation = emission $\pm$ bandwidth; second
7 order at each wavelength pair where emission = 2 $\times$ excitation
8 $\pm$ [2 $\times$ bandwidth]). The model was validated using split-half
9 validation and random initialization. Maximum fluorescence
10 values (F_{max}) are given for each component and summed to
11 total fluorescence (F_{tot}). The biological index (BIX; Huguet
12 et al. 2009) was also calculated as an indicator of the relative
13 contribution of autochthonous DOM.

14

Bacterial abundance

16   Water samples for bacterial abundance (4 mL) were fixed
17 with a filtered solution of paraformaldehyde (1% final concen-
18 tration) and glutaraldehyde (0.1% final concentration) after
19 adding a protease inhibitor (phenylmethanesulfonylfluoride
20 at a final concentration of 1 μmol L^{-1}), and kept frozen until
21 analysis (at $-20°$C in the field and $-80°$C back in the labora-
22 tory). Bacterial cells were counted by flow cytometry
23 (FACSCalibur, Becton–Dickinson). A solution of 0.94-μm fluo-
24 rescent beads (Polysciences) calibrated with trueCOUNT beads
25 (Becton–Dickinson) was added to each sample as an internal
26 standard to estimate cell abundance. Bacteria were labeled
27 with SYBR green I (Sigma-Aldrich) and counted for 2 min at a
28 low flow rate (12–15 μL s^{-1}).

29

Statistical analysis

31   The comparison among treatments was done for all DOM
32 descriptors and the bacterial abundance, in each pond sepa-
33 rately, using a two-way ANOVA with time (three levels, con-
34 sidered as fixed) and treatment (four levels, fixed). We
35 preferred not to perform a repeated measures ANOVA as
36 experimental conditions in ponds varied with time (experi-
37 ments were not synchronized). Normality and homogeneity
38 assumptions were checked by graphical examination of the
39 residuals. Among the 40 variables tested (10 descriptors $\times$ 4
40 ponds), seven could not be transformed to achieve these
41 assumptions (C5 in BYL1; DOC and C5 in BYL24; a_{320}, S_{285},
42 C2, and C3 in BYL38), for which we ran the Kruskal–Wallis
43 test, but results were very similar as for the ANOVA. When a
44 factor was significant, comparison of means among treatment
45 levels was done using Tukey HSD posthoc tests (or Tukey–
46 Kramer for the above-mentioned variables). Planned contrasts
47 were also used to compare absorption loss (see Table 4), and
48 bacterial growth (S vs. C, or B vs. BS). To explore the changing
49 patterns of DOM under the different treatments, principal
50 component analyses (PCAs) were applied on all DOM descrip-
51 tors available (DOC, a_{320}, S_{285}, peak fluorescence F_{max} of C1 to
52 C5, the sum of the five component F_{tot}, and biological index,
53 BIX) for each pond separately. The data were centered and
54 scaled to unit variance (excluding initial conditions presented

55 in Table 1). All univariate analyses were done using with JMP
56 Pro v.14, the PCAs were done using the *prcomp()* function
57 from R, and we used a significance level of α = 0.05 for all sta-
58 tistical analyses.

59

Results

Pond characteristics

63   The limnological characteristics of the studied ponds are
64 representative of the hundreds of polygonal and trough ponds
65 observed at the study site (Laurion et al. 2010). The limnologi-
66 cal characteristics of 11 polygonal ponds and 20 trough ponds
67 sampled in the same area in 2009 are presented in Table 1 for
68 comparison. In general, trough ponds have more nutrients
69 (TP, SRP, TN), DOM (DOC, a_{320}) and iron (Fe), and their DOM
70 was more colored (SUVA; see also section below for detailed
71 comparisons of DOM properties) as compared to polygonal
72 ponds. The colored waters of trough ponds sitting on ice
73 wedges promote highly stratified conditions throughout the
74 short summer, even though these water bodies are generally
75 less than 1 m deep. Partial mixing events are only occurring
76 during windy and cloudy days or at nights in trough ponds,
77 while coalescent polygonal ponds consistently have a well-
78 mixed water column; typical temperature profiles in coales-
79 cent pond BYL1 and trough pond BYL38 in the afternoon of a
80 sunny and calm day and of a cloudy and windy day are shown
81 in Fig. 1. Mixing rarely occurred below 0.6 m in BYL38 and
82 did not always occur at night, with the bottom temperature
83 remaining below $4°$C (on average $1.1°$C during the sampling
84 period as trough ponds lie over ice wedges). Low-center polyg-
85 onal ponds, such as BYL22, are very shallow (ca. < 30 cm
86 deep) and assumed to be well mixed as they are not wedged
87 into the topography, such as trough ponds, although their
88 thermal structure has not been assessed.

89

Environmental conditions during the experiment

91   Weather conditions during the experiment were variable,
92 with different combinations of sunny or cloudy days and with
93 periods of calm or high winds (Fig. 2). Incoming PAR varied
94 between 8 μmol photons m^{-2} s^{-1} during cloudy nights and
95 1342 μmol photons m^{-2} s^{-1} on bright sunny days (zenith at
96 13:00), and the overall photon flux received throughout the
97 experiment were similar among ponds ($\pm$ 6% of the average
98 total PAR received). Despite the fact that nights are not dark
99 in July at this latitude, the energy at wavelengths relevant for
100 DOM photolysis (UVR) gets very low. Therefore, about 85% of
101 the daily UV dose of a sunny day is received from 7 to 19 hr
102 (data obtained from Sequoia Scientific Inc. for a sunny day in
103 July; see Laurion and Mladenov 2013). Wind speed varied
104 between 0.3 and 9.7 m s^{-1} (average 3.1 m s^{-1}) and was 40%
105 lower at night (average 19:00–7:00 = 2.5 m s^{-1}) than during
106 the day (average 7:00–19:00 = 3.8 m s^{-1}). Air temperature var-
107 ied between $2°$C and $18°$C during the incubation period
108 (10–24 July). The water temperature at the incubation depth

Table 4. Initial rates of a_{320} changes (over the first 4 d) under the four treatments (C = filtered water in the dark; S = filtered water in sunlight; B = unfiltered dark; BS = unfiltered sunlight), with significant differences relative to control as indicated by a star ($p < 0.05$). Negative values indicate a loss of CDOM.
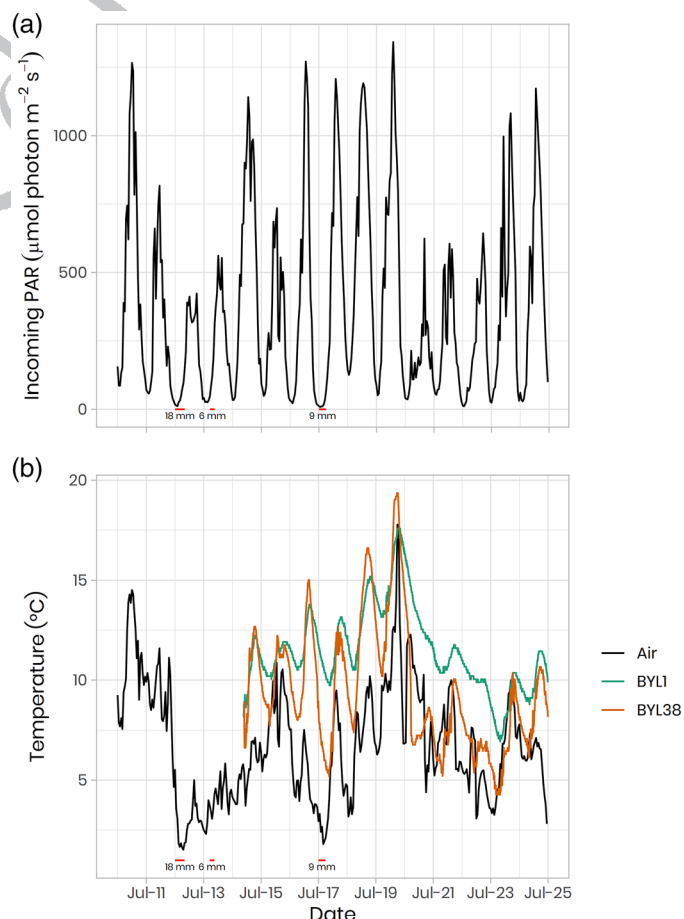
Treatment	BYL1	BYL22	BYL24	BYL38
	a_{320} change rate in m^{-1} d^{-1}			
C	−0.03 (− 0.2%)	−0.41 (− 2.0%)	−0.03 (− 0.1%)	−0.14 (− 0.2%)
B	0.07 (0.5%)	−0.87* (− 4.2%)	−0.66 (− 1.8%)	−4.53* (− 6.7%)
S	−0.33* (− 2.5%)	−0.69 (− 3.4%)	−0.46 (− 1.3%)	−0.72 (− 1.1%)
BS	−0.29* (− 2.2%)	−1.30* (− 6.3%)	−2.08* (− 5.7%)	−5.51* (− 8.2%)

(i.e., average temperature between loggers positioned at 0 and 10 cm used as a proxy for 5 cm depth) oscillated between 8°C and 18°C along the experiment in the coalescent pond BYL1, and between 5°C and 19°C in trough pond BYL38. Surface water temperatures were on average 2.3°C warmer in BYL1 than in BYL38, and about 0.7°C and 1.1°C cooler in the dark treatment than in the light treatment, respectively, for the two ponds. These differences likely reflected the incubation conditions for the other ponds BYL22 and BYL24 that have intermediate transparency.
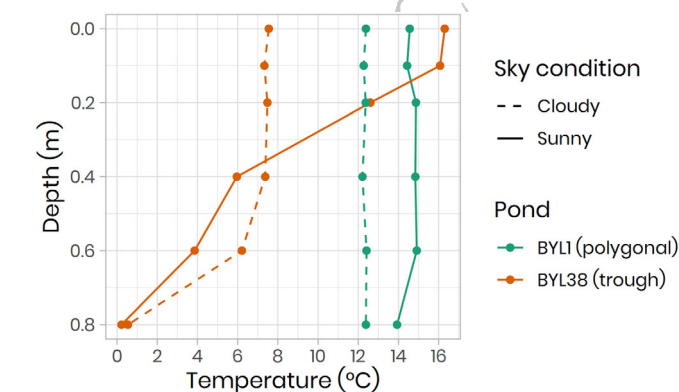
There were three major rain events locally recorded over the incubation period, on 12 July (18 mm), 13 July (6 mm), and 17 July (9 mm). The major rain event of 12 July occurred just before water sampling of BYL22, the last pond to be sampled, while the summer had been very dry before that (1.5 mm on 26 June, 0.5 mm on 7 July, and 1 mm on 11 July). The only other large rain event recorded that summer was on 13 August (31 mm), while total precipitation from 19 May to 18 August (the access period to this field site) was 85 mm of rain and 6 cm of snow. The climate normal based on 1981–2010 data provided by the meteorological station in Pond Inlet, located 85 km southeast of the study site, indicates a mean annual precipitation of 189 mm, with 91 mm falling in the form of rain (https://climate.weather.gc.ca/climate_normals/index_e.html).

Initial DOM properties of incubated waters

A gradient in DOM quantity and optical properties can be seen among the selected ponds. While DOC did not vary much (coefficient of variation CV, 15% for an overall average of 9.2 mg L^{-1}), a_{320} (a proxy for CDOM concentration) varied between 13.2 and 67.3 m^{-1} (CV 70%), generating wide-ranging absorptivity values (absorption per unit DOC) as

Fig. 1. Thermal profiles of polygonal pond BYL1 (green) and trough pond BYL38 (orange) on a sunny and calm day (18 July) and on a cloudy and windy day (20 July) at 16:00.

Fig. 2. (**a**) Incoming irradiance of the photosynthetically available radiation (PAR) with major rain events indicated by red lines (numbers indicate the amount of received rain), and (**b**) air temperature (black) and water surface temperature in BYL1 (green) and BYL38 (orange).

Table 3. Dissolved organic matter fluorescence properties of the four studied ponds at the beginning of the experiments extracted with PARAFAC, including the amount of each component (F_{max} of C1–C5) and the total fluorescence (F_{tot}) given in Raman units (RU). The percentage of each component to F_{tot} is given in parentheses. The first two columns indicate the excitation and emission peaks (and secondary peaks in parentheses) of each component.

PARAFAC components	Ex peaks (nm)	Em peaks (nm)	Description	BYL1 coalescent	BYL22 polygonal	BYL24 through	BYL38 through
				Fluorescence RU (%)			
C1	< 250 (320)	440	Microbial fulvic-like*	0.37 (31)	0.35 (36)	0.88 (46)	1.27 (49)
C2	< 250 (300)	390	HMW humic-like[†]	0.24 (20)	0.18 (19)	0.30 (16)	0.44 (17)
C3	< 250 (360)	422	Humic-like[‡]	0.21 (17)	0.15 (16)	0.33 (17)	0.33 (13)
C4	270 (380)	492	Terrestrial fulvic-like[§]	0.11 (9)	0.10 (10)	0.25 (13)	0.36 (14)
C5	280	334	Microbial tryptophan-like[‖]	0.27 (23)	0.18 (19)	0.13 (7)	0.19 (7)
F_{tot}	—	—	—	1.20	0.97	1.89	2.58

HMW, high molecular weight.

*Fulvic-like molecules potentially of a microbial origin as shown in Murphy et al. (2008) for their C2 (EX/EM 315/418), or in Guillemette and del Giorgio (2012) for their C1 (350/450).

[†]Similar to humic-like component U 250(320)/370, found to be widespread but highest in wetlands and forested environments, very labile and associated with freshly produced DOM in Fellman et al. (2010); also similar to microbial humic component C6 (<250(285)/386) in Williams et al. (2013).

Q7 [‡]Similar to humic-like peak C (320–360/420–460) in Coble et al. (1990); also similar to humic-like C1 (240-320/428) in Stedmon et al. (2003).
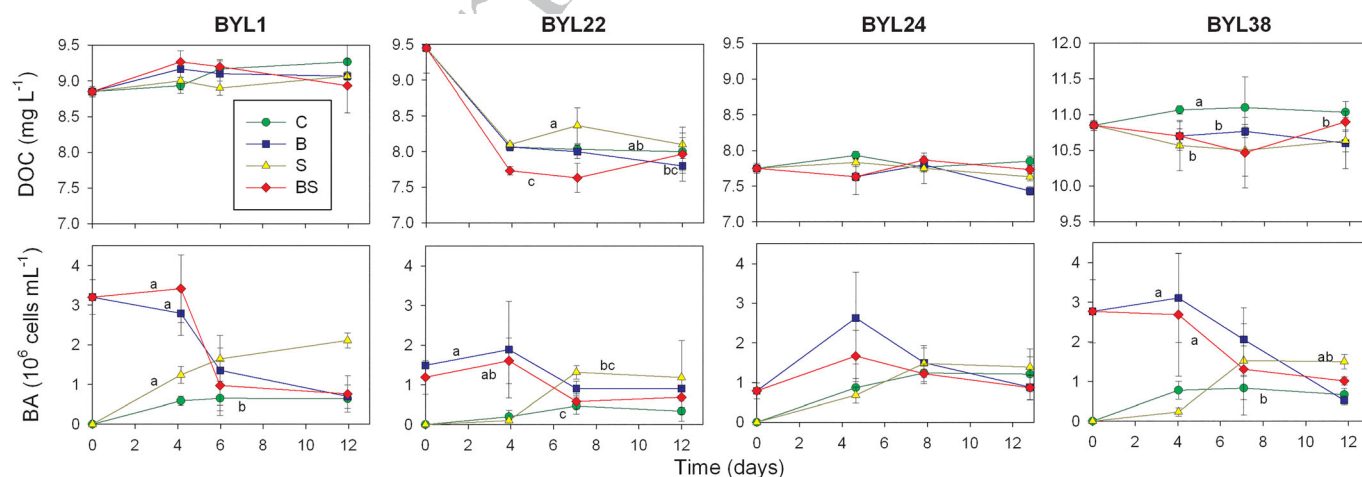
[§]Fulvic-like molecules of a terrestrial origin and widespread, similar to C3 (260(370)/490) in Murphy et al. (2008).

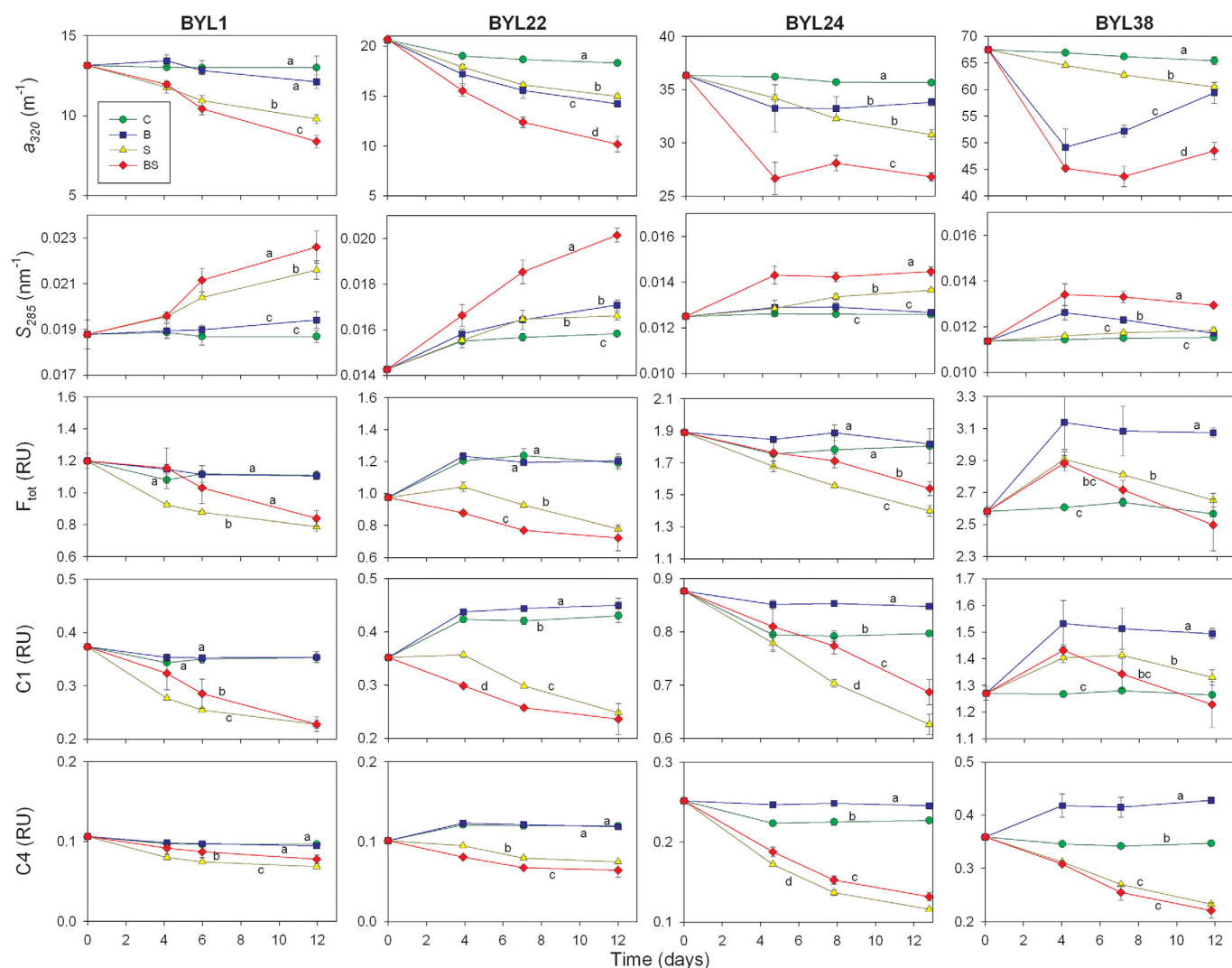[‖]Similar to tryptophan-like component (270–280/330–368) in Fellman et al. (2010).

illustrated by the SUVA index (Table 1). Trough ponds are characterized by higher CDOM (a_{320}) and more colored DOM (SUVA) as compared to polygonal ponds. Dissolved iron (Fe) also varied widely among ponds, the highest value observed in the eroding trough pond BYL38 (3.05 mg L^{-1}), which is known to affect DOM optical properties (Poulin et al. 2014). Even if part of DOM color comes from its interaction with Fe, the corrected SUVA values remain higher in trough ponds than in polygonal ponds (values in parentheses). The lower absorption slopes (S_{285}) and higher SUVA

values together indicate the presence of larger, more aromatic molecules in the DOM pool of trough ponds affected by soil erosion, although the proportion of DOM leached from recently eroded permafrost soils was not determined in the present study.

The EEMs also reveal higher FDOM in trough ponds, with components corresponding to previously identified fluorophore groups (Table 3). Trough ponds had a larger fraction of fulvic-like C1 (> 46% of F_{tot}) and a smaller fraction of tryptophan-like C5 (7%) as compared to the polygonal ponds

Fig. 3. Experimental changes in average (± SD) dissolved organic carbon (DOC; first row of panels) and bacterial abundance (BA; second row) over 12 d of incubation under four treatments (C = filtered water in the dark; S = filtered water in sunlight; B = unfiltered dark; BS = unfiltered sunlight), for the coalescent polygonal pond BYL1, polygonal pond BYL22, stabilized trough pond BYL24 and erosive trough pond BYL38. Although the scale range may vary among ponds, the y-axis increments are consistent for each parameter shown. The different letters indicate the significant differences between treatments according to a Tukey HSD or Tukey–Kramer multiple comparison.

Fig. 4. Experimental changes in average ($\pm$ SD) DOM color (a_{320}; top panels), absorption spectral slope at 285 nm (S_{285}; second row of panels), total DOM fluorescence obtained from the EEMs (F_{tot}; third row), and of most dynamic fluorescent components C1 (fourth row) and C4 (fifth row) over 12 d of incubation under four treatments (C = filtered water in the dark; S = filtered water in sunlight; B = unfiltered dark; BS = unfiltered sunlight), for the coalescent polygonal pond BYL1, polygonal pond BYL22, stabilized trough pond BYL24 and erosive trough pond BYL38. Although the scale range may vary among ponds, the *y*-axis increments are consistent for each parameter shown. The different letters indicate the significant differences between treatments according to a Tukey HSD or Tukey–Kramer multiple comparison.

(< 36% of C1 and > 19% of C5). The coalescent polygonal pond BYL1 presented the highest quantity of Component C5 (0.27 RU, or 23%); this pond also showed the highest BIX value (attributed to a larger fraction of autochthonous DOM; Huguet et al. 2009). While varying amounts of C2, C3, and C4 were found within the four ponds, their proportions were relatively similar among ponds, with differences always remaining below 5%. It is only Components C1 and C5 that varied substantially among ponds initially.
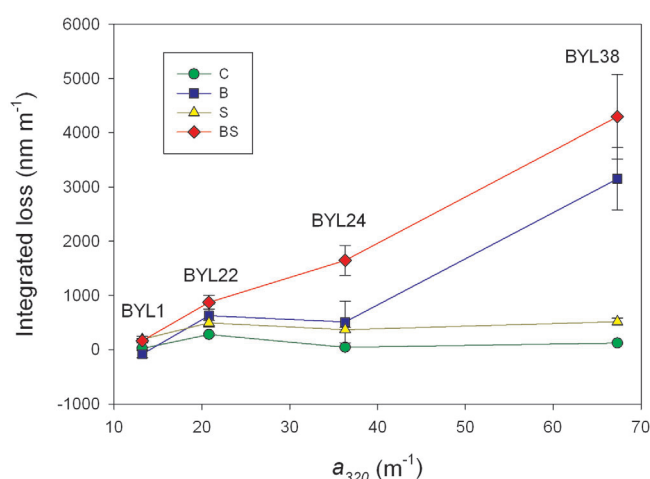
Treatment effects on microbial abundance and DOC

The filtered (S and C) water treatments showed increases in bacterial counts after a few days (Fig. 3). This bacterial regrowth was higher under sunlight than in the dark (control)

for BYL1, BYL22, and BYL38 (planned contrast on S and C treatments only; $p < 0.018$). In unfiltered treatments (B and BS), a decrease in bacterial abundance over 12 d was rather observed, potentially caused by microzooplankton grazing or competitive interactions under the experimental conditions. There was no significant difference in bacterial abundance patterns between B and BS treatments (planned contrast on B and BS treatments only; $p > 0.166$), and the final bacterial abundance seems to converge among treatments.

Overall, the DOC did not change significantly over the 12 d of incubation in any of the treatments (Fig. 3; $p > 0.152$ on time effect; Table S1), with a CV of less than 5% among all treatments and replicates of any specific pond (less than 3% when excluding the time zero of BYL22 for which the

Fig. 5. Integrated CDOM absorption losses (average ± SD) after 4 d of incubation under four treatments (C = filtered water in the dark; S = filtered water in sunlight; B = unfiltered dark; BS = unfiltered sunlight) as a function of initial CDOM (a_{320} used as a proxy on the X-axis) in the four studied ponds. The integrated loss was calculated as the area under the curve of a (λ) at time zero minus a (λ) after 4 d.

incubation water was collected after heavy rainfall on 12 July; see discussion for this case). Only was there a treatment effect detected for BYL38 ($p = 0.011$) and BYL22 ($p = 0.0004$), but with differences among treatments of less than 0.4 mg L^{-1}. The precision of the TOC analyzer (quantification limit of about 0.5 mg L^{-1}) was not high enough to resolve the subtle changes that occurred at this site over the experimental time frame. Therefore, despite CDOM becoming less colored over time (see below), neither the microbial (Treatment B) nor the photochemical (Treatment S) transformation of DOM, and not even the microbial consumption of the photoproducts (included in treatment BS), generated significant mineralization of DOM into CO_2.

Treatment effects on CDOM

Sunlight (Treatment S) generated a loss of color over time, as expressed by the decrease of a_{320} (top panels in Fig. 4), with higher (in BYL1), comparable (in BYL22 and BYL24) or lower loss rates (in BYL38) than those caused by microbial degradation (Treatment B). In treatments containing the original biomass of bacteria at time zero (B and BS), complex dynamics were observed in trough ponds BYL24 (CDOM loss slowing down) and BYL38 (CDOM increasing after an initial loss). The absorption slope S_{285} increased over time with a plateauing (BYL24) or reversing trend (BYL38). The two-way ANOVA performed on a_{320} and S_{285} indicate significant treatment effects ($p < 0.0002$; details provided in Supporting Information Table S1).

A comparison of the initial change rates over 4 d of incubation (at the first subsampling date; Table 4) minimizes the confounding effect caused by this bacterial regrowth in the S treatments (Fig. 3) and avoids the complex DOM production
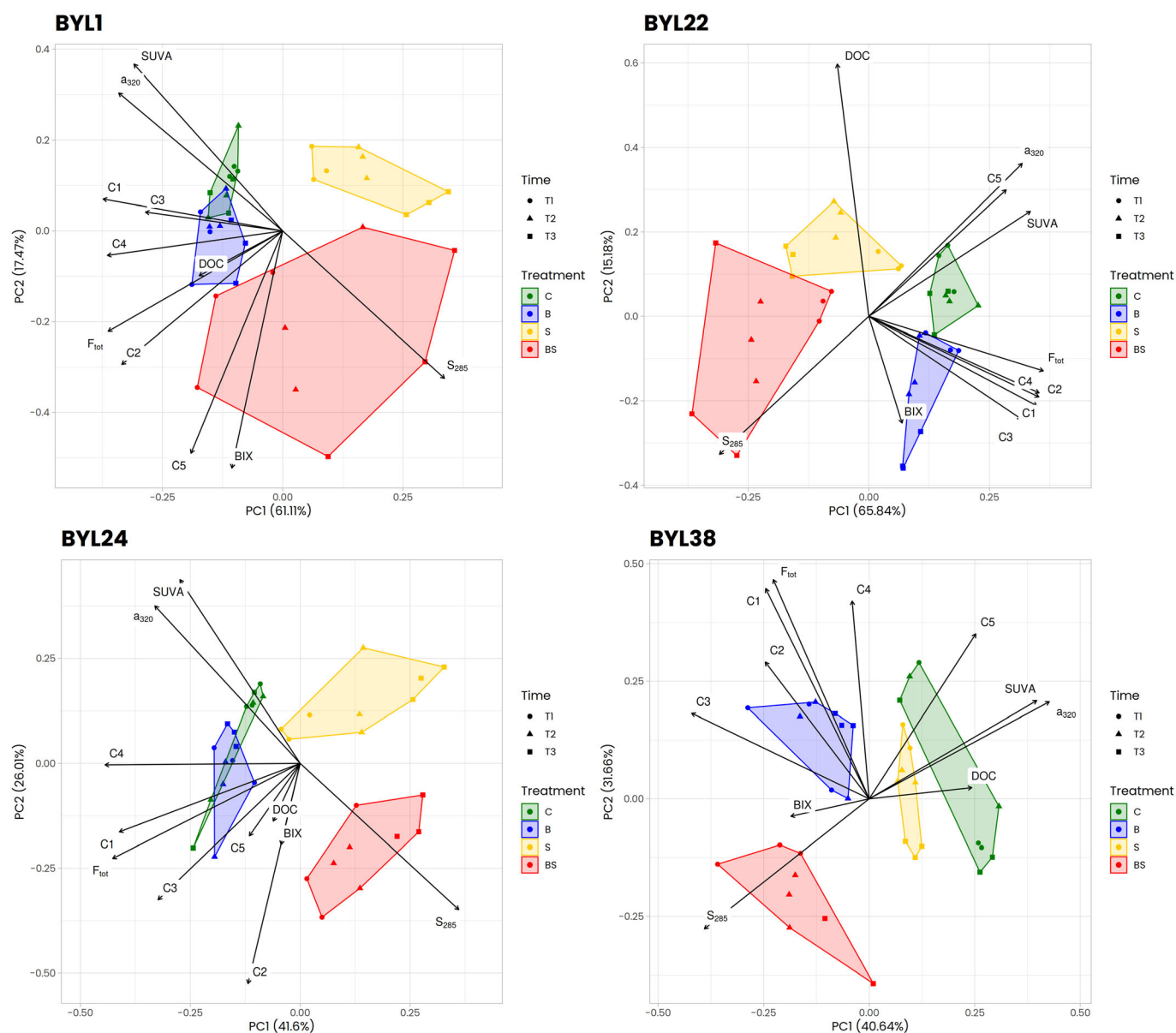
dynamics sometimes occurring thereafter (e.g., the decrease in a_{320} of BYL38 reversing after 4 d; Fig. 4). These results indicate that microbial degradation caused a decrease of a_{320} at a rate varying from 0.5% d^{-1} (BYL1) to 6.7% d^{-1} (BYL38), which was always higher than in the control treatment (significant at $p < 0.05$ for BYL22 and BYL38). On the other hand, photobleaching rates varied from 1.1% d^{-1} (BYL38) to 3.4% d^{-1} (BYL22), or from 0.33 m^{-1} d^{-1} (BYL1) to 0.72 m^{-1} d^{-1} (BYL38) for the amount of color lost per day (at 320 nm). The concomitant effect of sunlight and microbes (BS) presented the highest rates reaching 8.2% d^{-1} in through pond BYL38 (absolute loss rate also highest in this pond). The concomitant loss was larger than the sum of B and S losses only in trough pond BYL24.

To assess the spectral loss of DOM color, we integrated from 250 to 700 nm the loss of absorption after 4 d of incubation (Fig. S1). There was a significant treatment effect on this integrated short-term loss for all four ponds ($p < 0.0005$), with treatment BS generally showing the highest losses. When normalized to the area below the initial absorption curves, this integrated loss over 4 d for treatment BS varied from 6% (in coalescent pond BYL1) to 36% (in trough pond BYL38). Interestingly, the integrated loss increased as a function of initial CDOM (a_{320} used as a proxy for the quantity of CDOM) for B and BS treatments but did not change with CDOM for the S treatment (and C; Fig. 5).

Treatment effects on FDOM and overall DOM trends

By contrast, the metrics for FDOM (F_{tot}, C1 and C4 shown in Fig. 4, other PARAFAC components can be found in Supporting Information Fig. S2, and all data are available in repository Laurion et al. 2020) did not follow the same patterns as absorption, especially in the presence of microbes where F_{tot} generally increased (BYL22, BYL38) or remained constant (BYL1, BYL24). F_{tot} decreased under sunlight (S and BS) in most ponds, as did the a_{320} values, but this was not seen in trough pond BYL38 where only C4 decreased with sunlight, while C2 and C3 presented an increasing trend. Overall, Component C5 did not show any clear patterns, except in coalescent pond BYL1 where it slightly decreased under sunlight, similar to the other four components. The highest loss rate in FDOM was observed for C1 in trough pond BYL24 (0.25 RU lost over 12 d under S treatment, or 29% loss).

Principal component analyses (PCA) were applied on all DOM properties measured along the experiments (excluding measurements at time zero; Fig. 6). From 68% to 81% of the variance was explained by the first two components, depending on the ponds. The PCA shows a unique DOM signature among treatments for all four ponds, with little overlapping of the polygons defined by time subsamples, suggesting that the four treatments produced DOM pools with distinctive characteristics. Subsamples of treatment BS (red) show the largest dispersal in DOM properties, while control

Fig. 6. Principal component analyses for the four ponds including all DOM variables and using the same color code as in Figs. 3–5. Each data point represents the DOM signature of a bottle replicate at a subsampling time (excluding time zero). Replicates are distinct and different symbols are used for subsampling done after about 4 d (circles), 8 d (triangles), and 12 d (squares).

subsamples (green) were closest to each other. Trough pond BYL38 was an exception again, with the sunlight treatment showing the narrowest change over time (yellow).

Discussion

Limited pelagic mineralization of DOM in small tundra ponds

Some studies have explored the microbial mineralization of permafrost organic matter using dark incubations (reviewed by Vonk et al. 2015), while others focused on its

photochemical decay using natural or artificial radiation (e.g., Cory et al. 2013; Laurion and Mladenov 2013; Stubbins et al. 2017). Studying the combined effects of microbial and light degradation processes is important because they are occurring concurrently in aquatic ecosystems, but such studies are scarce for Arctic regions (Ward et al. 2017; Shirokova et al. 2019). This simultaneous interaction influences the fate of DOM along the aquatic continuum and may affect the transfer of ancient C stocks to the atmosphere (Cory and Kling 2018) or to coastal waters. However, the tundra ponds considered in this study presented undetectable DOC losses

and therefore low mineralization of DOM into CO_2 under natural conditions. This was the case when both microbes and sunlight were acting independently (treatments B or S) and concurrently (BS). It means that neither direct photomineralization of DOC nor the microbial mineralization of DOM photoproducts were high enough to be statistically significant over 12 d. These observations also apply to a pond deeply affected by permafrost thermoerosional processes (trough pond BYL38) and receiving aromatic C (higher CDOM and SUVA) from the surrounding peaty soils during the thawing season. On the other hand, transformation of the DOM pools clearly occurred (see the section below on "Transformation of DOM related to mixing regime and historical decay").

The limited DOM mineralization obtained in the present study applies to water that was sampled on 10–12 July from the pelagic zone of the ponds, not long after ponds have finished melting (extending from 15 to 30 June), and at the beginning of the warming period extending over July at this site (based on water thermal profiles; unpublished results). The period before 10 July was very dry (2 mm of rain recorded locally since 19 May), and thus DOM inputs to ponds were limited in previous weeks. It is possible that the OC leaching earlier during the snowmelt period, or after large rain events and as the active layer deepens later in the season, would present higher mineralization rates. Studies acknowledge the importance of considering seasonality when studying DOM bacterial and photochemical mineralization in rivers (Mann et al. 2012) or in lakes (Vachon et al. 2016). Because small tundra ponds have stagnant waters, small volume and dominant littoral zones, the DOM pool of these water bodies is likely very responsive to rain events and previous light exposure. Such responses have been shown for a subarctic polymictic lake (Gibson et al. 2001) and other larger lakes (Catalán et al. 2016).

Other studies have presented reduced or nondetectable DOM mineralization (i.e., DOC loss) in frozen peat bogs (showing low photolability and biolability; Shirokova et al. 2019) or Yedoma permafrost leachates (showing low photolability; Stubbins et al. 2017). The biolability of soil organic matter from northern Eurasia (including yedoma, cryoturbated soils and peatlands; Kuhry et al. 2020) and interior Alaska (Wickland et al. 2018) was also considered relatively low. This is quite different from what was observed in other studies, where sometimes high mineralization rates were reported along the aquatic continuum or from permafrost leachates (Cory et al. 2013; Vonk et al. 2013; Drake et al. 2015; Mann et al. 2015). These discrepancies in DOM mineralization rates across the Arctic need to be better understood before upscaling exercises provide meaningful estimates (Koehler et al. 2014). Discrepancies are likely driven by differences in the parent material leaching into aquatic systems (e.g., its organic content, the transformation of organic matter before and during its incorporation into permafrost), the historical exposure to microbial and photochemical degradation (time since thaw, water residence time) and the physicochemical conditions of receiving water bodies (e.g., morphology, mixing and light regimes, pH), all affecting the molecular composition of the DOM pool examined at a specific time, and thus its reactivity (Abbott et al. 2014). For example, the rapid biomineralization of Pleistocene-age permafrost C leached from Yedoma soils was highly linked to the presence of low-molecular-weight, hydrogen-rich aliphatic compounds, quickly disappearing after entering the hydrologic network (Drake et al. 2015), and underlining the importance of considering C cycling at the landscape scale. It is worth mentioning that some of the divergence among studies could also be linked to variations in the definition of lability and in the chosen experimental setup. For example, variable filtration efficiencies in removing microbes or variable incubation lengths can lead to differing microbial regrowth or taxonomic composition that can affect the outcome of lability assays (Dean et al. 2018).

What is important to underline is that the low pelagic DOM mineralization observed here corresponds to a relatively cold moment on the tundra (i.e., a moment of reduced organic matter movement and processing). Such cold moments can potentially be under-represented in the literature and highly dependent on precipitation regimes. As pointed out by Wen et al. (2020), catchments serve as producers and storage reservoirs for DOM under hot and dry conditions, and transition into DOM exporters under wet and cold conditions. The predicted increase in annual precipitation for Arctic tundra regions, particularly in winter and fall (Bring et al. 2016), will control DOM export to aquatic ecosystems and the balance between autochthonous/allochthonous sources (Osburn et al. 2019), which will certainly affect seasonal patterns in DOM mineralization.

The photostimulation of bacterial growth

The absence of significant DOM mineralization does not mean sunlight was not affecting DOM and microbes. One noteworthy aspect of our results is the observed stimulation of bacterial growth after the water has been filtered and exposed to sunlight (treatment S vs. C in Fig. 3 last row). Even though $0.2\text{-}\mu m$ filtration has been extensively used to sterilize water, this step can leave cells behind, generating a bias when the goal is to isolate photochemical from biological effects. Therefore, special care should be taken when filtering water, and cell abundance always controlled. Beyond this problem, the stimulated growth of bacteria left behind observed here suggests that cells were benefiting from the exposure to sunlight. Such stimulation has been reported in various aquatic systems (e.g., Lindell et al. 1995; Wetzel et al. 1995; Miller and Moran 1997).

In general, bacterial growth stimulation by sunlight is attributed to the production of smaller, more aliphatic and oxidized molecules by hydroxyl radical reactions or other

photoreactions (Ward et al. 2017). The photochemical release of nutrients from DOM could also be involved (Vähätalo et al. 2003). Interestingly, Ward et al. (2017) have shown that sunlight significantly increased microbial respiration when photo-alteration produced molecules that native microbial communities used prior to light exposure, but the contrary also occurred (decreased respiration when photo-altered products were not *familiar* to native communities). On the other hand, we cannot exclude that part of the growth stimulation observed in the present study under sunlight was linked to the slightly higher temperature caused by the absorption of heat by water (on average 0.7°C higher for coalescent pond BYL1, and 1.1°C higher for trough pond BYL38), a potential indirect effect that also deserves attention.

The bacterial growth in filtered treatments could only be detected in the absence of protozoan predation and under the reduced competition that occurred after the microbial population was significantly removed by filtration. Considering the small C content of a few millions of bacterial cells (totaling $\ll 1$ mg C L^{-1} even considering large bacteria, conversion factors available in the literature, and a fraction lost through respiration), the absence of any significant decrease in DOC despite the bacterial stimulation observed here is plausible over the time frame of the experiment. For example, recent studies revealed the widespread occurrence of candidate phyla radiation bacteria that are very small cells (< 0.2 μm; Castelle et al. 2018), not removed by conventional filtration, and with a role yet to be defined. Further research involving molecular tools and bacterial production are needed to more directly evaluate the biolability of differing DOM pools and better inform future experimental design.

Transformation of DOM related to mixing regime and historical decay

This study shows that four nearby tundra ponds can have different patterns in DOM photochemical and microbial transformation, which are likely driven by the quality of the DOM pool at the start of the experiment. This is in agreement with results from studies in subarctic lakes showing changes in composition and biological reactivity along DOM gradients (e.g., Berggren et al. 2019). Notably, the photodegradability of DOM has proven to be related to its color (Lapierre and del Giorgio 2014). In the present study, the fastest losses in color were indeed observed in the most colored pond (erosive trough BYL38; Tables 1 and 4).

Around 10% to 27% of CDOM (a_{320}) was lost after 12 d of incubation under sunlight, with slower, similar, or faster photochemical decay than the microbial decay (7%–31% loss; Fig. 4). This was accompanied by an inverse rising trend in absorption slopes at short wavelengths (illustrated by S_{285}). Photochemical alteration was shown to produce less colored DOM in Arctic lakes and rivers (e.g., Mann et al. 2012; Cory et al. 2014). CDOM losses accompanied by rising absorption slopes and little or no production of CO_2 (or limited DOC

losses) is called partial photooxidation, and is usually attributed to the transformation of aromatic or high-molecular-weight DOM into aliphatic or lower-molecular-weight compounds (Cory and Kling 2018). Although photo-altered DOM molecules through partial photooxidation were previously shown to accelerate the microbial processing of permafrost DOM (e.g., Cory et al. 2013; Ward et al. 2017), this was not significant in the studied ponds since BS treatments were not showing significant DOC losses despite marked changes in CDOM and FDOM. Nonetheless, the bacterial regrowth observed under sunlight suggests that partial photooxidation may have occurred and may stimulate DOM mineralization to a varying extent, depending on the mixing regime that controls sunlight exposure and water temperature.

The studied water bodies present different mixing regimes. Coalescent pond BYL1 is a well-mixed system of less than a meter deep, efficiently exposing its DOM to elevated irradiance. Therefore, when this pond was sampled after a long period of dry conditions, it presented the lowest SUVA index among the four ponds (Table 1) and a particularly slow photodecay rate (see the CDOM loss rates for S treatment in Table 4). The measured rate might even be overestimated since maintaining bottles at the surface was artificially increasing the irradiance dose for this well-mixed pond. The same pond was studied during the previous summer under similar incubation conditions but 1 week later (18–31 July 2009; Laurion and Mladenov 2013), and results indicate that CDOM photodecay was slightly faster (0.46 m^{-1} d^{-1} in 2009 as compared to 0.33 m^{-1} d^{-1} in the present study). In this specific example, 16.5 mm of rain had fallen over the 2 weeks preceding the experiment in 2009, as compared to 2.0 mm in 2010, putatively transporting more DOM freshly leached into the pond, which may explain the faster photodecay. Moreover, incident radiation was 64% lower in 2009 as compared to 2010 over the 2 weeks preceding the experiment (but with similar radiation during the experimental days; CEN 2018), lowering the historical photodegradation of the DOM pool (i.e., before it was sampled). Therefore, the weather condition previous to water sampling is a critical aspect of any experimental assessment that needs to be taken into account.

In the other three cases, maintaining bottles at the surface may well reflect the in situ conditions (at the surface) as the ponds are either very shallow (polygonal pond BYL22) or stably stratified in July (trough ponds BYL24 and BYL38). Partial mixing of the water column (mainly observed at night; unpublished data), however, renews water masses at the surface to a certain extent. Because exposure to sunlight at depth is limited in colored waters, longer residence time combined with periodic mixing should favor DOM removal at the scale of a lake or along the river continuum (Cory et al. 2014; Groeneveld et al. 2016). In this context, we expected that pond BYL22 would have presented a similarly low decay rate as BYL1 considering its shallowness (~ 0.2 m) and the previous exposure of its DOM pool to an overall high irradiance, but

instead high CDOM loss under sunlight was observed (similar to BYL38; Fig. 4; Table 4). Pond BYL22 was however sampled 1 d later than the other three, right after a heavy rainfall event (18 mm). This likely brought in fresh leachates of DOM. Many studies have shown a positive correlation between precipitation and CO_2 emissions or photochemical mineralization of DOM (e.g., Rantakari and Kortelainen 2005; Suhett et al. 2007; Groeneveld et al. 2016). In the case of BYL22, the starting DOM properties (not particularly chromophoric or fluorescent, see SUVA and F_{tot} in Tables 1 and 3) and the sharp decrease in DOC observed at the start of the experiment for all treatments (Fig. 3) suggests that the rain event leached uncolored DOM that may be prone to flocculation under the pelagic conditions of this pond, although it is colored DOM flocculation that was previously observed (e.g., von Wachenfeldt and Tranvik 2008). Alternatively, we cannot exclude the possibility that the DOC quantification at time zero was biased (no replicate). This pattern needs to be confirmed by paying more attention to DOM properties before and after rain events, controlling with direct measurements of CO_2 and flocculates, and using methods that also characterize the nonchromophoric fraction of DOM. The DOM composition in such small water body (volume < 15 m^3 for BYL22, while BYL1 was > 150 m^3) is likely very dynamic, but this is rarely assessed as we generally tend to aim for larger, less ephemeral water bodies. Yet, large quantities of DOM may still be mineralized in these water bodies at the landscape scale, and to account for this, better spatiotemporal coverage is needed.

DOM recycling in small tundra ponds

Significant CDOM losses were also observed in dark incubations (B treatments), but these losses cannot be clearly associated with microbial mineralization since they were not accompanied by substantial DOC losses, unless recycling was very efficient. It was rather linked to a microbial conversion of molecules, and these were apparently fluorescent compounds in ponds BYL22 and BYL38 (B treatment in Fig. 4). Substantial production of C1 compounds, a group of humic-like molecules previously associated with DOM of a microbial origin (Murphy et al. 2008), was observed in these two ponds. The consumption of chromophoric/aromatic molecules concurrent with a production of fluorescing molecules was also found in lacustrine systems of the temperate zone, and largely depended on DOM source (Guillemette and del Giorgio 2012). The production of CDOM and FDOM has also been observed in laboratory incubations of subarctic lake DOM (Berggren et al. 2019). Bacteria tend to be presented in the literature as low-molecular-weight nonaromatic DOM consumers, with photodegradation often causing DOM properties to shift in an opposite direction than biodegradation (Hansen et al. 2016). These general trends may be inadequate for thermokarst lakes deeply affected by permafrost soil erosion, receiving organic matter with different reactivities to microbial and

photochemical degradation than allochthonous matter from nonpermafrost regions or from regions not affected by thermokarstic erosion. Moreover, as pointed out by Berggren et al. (2019), the common assumption that CDOM has a terrestrial origin may need to be revised.

Overall, the PCA analysis indicates that presence of the complete microbial community (unfiltered) clearly generated changes in the composition of fluorophores, while sunlight was particularly driving changes in DOM molecular size (absorption slope). In particular, eroding trough ponds such as BYL38 may be deeply influenced by soil microbial assemblages specialized in processing large aromatic molecules (see details on bacterial assemblages in Negandhi et al. 2014, where the term runnel pond was used instead of trough ponds). Roth et al. (2019) concluded that plant material is extracellularly decomposed to smaller molecules, which are then consumed and, in part, mineralized or transformed to larger microbial-derived molecules forming a secondary pool of organic matter (potentially more fluorescent). The reverse trend in CDOM observed along the 12-day incubation in BYL38 (i.e., a decrease in CDOM followed by an increase) might have resulted from such a turnover dynamic. Extracellular decomposition in ponds from enzymes produced in nearby soils could also help explain the absence of significant DOC mineralization despite clear CDOM changes. Moreover, microbial degradation was more effective than photodegradation in BYL38, suggesting a higher proportion of bioreactive molecules or a more efficient microbial community eroded from soils (Ward et al. 2017). In the PCA, BYL38 (lowest transparency) showed the narrowest changes in DOM properties for S treatment (Table 1, Fig. 6). The CDOM losses integrated over the first 4 d of incubation and plotted as a function of initial CDOM (Fig. 5) increased for treatments with bacteria (B and BS) but not under filtered sunlight or control treatments (S and C). This suggests that conditions in colored trough ponds are leading to a particularly dynamic transformation of the DOM pool, potentially linked to the import of native soil microbes. Molecular-level characterization of DOM (e.g., with ultrahigh-resolution mass spectrometry, nuclear magnetic resonance spectroscopy or pyrolysis-gas chromatography–mass spectrometry; Lennon et al. 2013; Roth et al. 2019) is needed to further explain differences among ponds, but they are likely linked to the relative inputs by benthic primary producers and eroding peaty soils. Since both of these DOM sources will respond to climate change through different mechanisms (Osburn et al. 2019), their transformation and fate need to be explored in more detail and with consideration of microbial food web interactions.

The dominance of benthic CO_2 production

Previous studies on trough ponds at this site (including BYL24 and BYL38) showed that these water bodies are most often largely supersaturated in CO_2 in July (Laurion et al. 2010; Bouchard et al. 2015), with surface concentrations reaching

up to 619 μM (median = 50 μM, n = 225 for 31 ponds; unpublished results). Therefore, the slow DOM mineralization rates observed in the present study suggest that most of the CO_2 produced during the peak summer season is rather associated to benthic OM processing such as shown in small boreal lakes (Kortelainen et al. 2006), and/or to lateral transport of adjacent soil pore water (Campeau et al. 2018). There was a net production of CO_2 when surface sediments of the same four ponds were incubated over a few days in the dark, and faster production in trough ponds compared to polygonal ponds (particularly for BYL38; see Table 2 in Negandhi et al. 2016). This result indicates that particulate OM deposited at the bottom of these water bodies, either through permafrost erosion, DOM flocculation or primary production, is biolabile. Determining the fate of these different sources of OM under the projected summer lengthening, stratification strengthening and altered precipitation regime will be particularly relevant to climate modelers as they would not generate the same feedback onto climate.

Conclusions

DOM mineralization in the pelagic zone of isolated tundra ponds was not significant at the present study site, contrary to what was found in permafrost leachates, headwater creeks or rivers of other Arctic regions. Differing parent material among sites (permafrost extent, ice content, historical deposition, diagenesis, relief; Tank et al. 2020) potentially generates diverse assemblages of molecules with a wide range of bio- and photoreactivity, but the difference is also likely linked to the moment when water was sampled. In the present study, it happened to follow a dry period of many weeks. Although the DOM pool in these light-exposed water bodies appeared very reactive, the quantum yield for photochemical mineralization of DOC was apparently not high. There are potentially other moments during the short Arctic summer, including early spring and after rainfall events, when ponds receive pulses of DOM leaching from surrounding soils with a higher mineralization potential. The static nature of tundra ponds during summer, with their long water retention time, may thus constrain hot moments (i.e., periods of intense mineralization) when water moves and transports C on the landscape, otherwise pelagic DOM mineralization rapidly reaches stable state.

Tundra ponds can dominate the landscape in certain regions and are exposed to increasing radiation as summers lengthen. They are also facing dynamic changes in the amount of ancient and modern C they receive as permafrost thaws and plants grow. The contrasting results on the effects of sunlight on DOM mineralization seen in the literature merit further assessments over a wider range of water body types and landscapes, while accounting for the age of mineralized C pools. These assessments will need to exploit recent methodological approaches to characterize DOM and microbes in a more holistic approach and exploit isotopic

tracers to decipher current C pathways and make reliable projections as the climate changes.

To account for the effect of sunlight on permafrost C mineralization in freshwaters and scale this up, assessments need to be done (1) under natural sunlight exposure considering the mixing regime that can be quite different among tundra ponds and compared to larger lakes and rivers, (2) along the open-water season accounting for rain events and active layer deepening, and (3) controlling for bacterial abundance and DOM flocculation. Working in situ with an experimental approach has many advantages: it allows for the use of natural sunlight that is complex to mimic, and it minimizes changes in microbial assemblages and DOM prior to starting the experiments. Lab conditions are well suited to working on leachates from peat cores or vegetation materials that can be kept frozen for later experiments. Efforts should be given to applying standardized protocols (e.g., Vonk et al. 2015) but considering the logistical constraints associated with sampling in the Arctic. Although there are challenges associated with studying C mineralization in remote Arctic regions, the strong rates and contrasting trends observed among the few regions studied and the huge C stock involved call for urgency to improve future projections.

References

Abbott, B. W., J. R. Larouche, J. B. Jones, W. B. Bowden, and A. W. Balser. 2014. Elevated dissolved organic carbon biodegradability from thawing and collapsing permafrost. J. Geophys. Res. Biogeosci **119**: 2049–2063.

Abnizova, A., J. Siemens, M. Langer, and J. Boike. 2012. Small ponds with major impact: The relevance of ponds and lakes in permafrost landscapes to carbon dioxide emissions. Global Biogeochem. Cycles **26**: GB2041.

Berggren, M., C. Gudasz, F. Guillemette, G. Hensgens, L. Ye, and J. Karlsson. 2019. Systematic microbial production of optically active dissolved organic matter in subarctic lake water. Limnol. Oceanogr. **65**: 951–961.

Bogard, M. J., and others. 2019. Negligible cycling of terrestrial carbon in many lakes of the arid circumpolar landscape. Nat. Geosci. **12**: 180–185.

Bouchard, F., and others. 2015. Modern to millennium-old greenhouse gases emitted from ponds and lakes of the Eastern Canadian Arctic (Bylot Island, Nunavut). Biogeosciences **12**: 7279–7298.

Bring, A., and others. 2016. Arctic terrestrial hydrology: A synthesis of processes, regional effects, and research challenges. J. Geophys. Res. Biogeosci **121**: 621–649.

Campeau, A., and others. 2018. Stable carbon isotopes reveal soil-stream DIC linkages in contrasting headwater catchments. J. Geophys. Res. Biogeosci **123**: 149–167.

Castelle, C. J., C. T. Brown, K. Anantharaman, A. J. Probst, R. H. Huang, and J. F. Banfield. 2018. Biosynthetic capacity,

metabolic variety and unusual biology in the CPR and DPANN radiations. Nat. Rev. Microbiol. **16**: 629–645.

Catalán, N., R. Marcé, D. N. Kothawala, and L. J. Tranvik. 2016. Organic carbon decomposition rates controlled by water retention time across inland waters. Nat. Geosci. **9**: 501–504.

Centre for Northern Studies (CEN). 2018. Climate station data from Bylot Island in Nunavut, Canada, v. 1.8 (1992–2017). Nordicana: D2. doi:10.5885/45039SL-EE76C1BDAADC4890

Coble, P. G., S. A. Green, N. V. Blough, and R. B. Gagosian. 1990. Characterization of dissolved organic matter in the Black Sea by fluorescence spectroscopy. Nature **348**: 432–435.

Comyn-Platt, E., and others. 2018. Carbon budgets for 1.5 and 2°C targets lowered by natural wetland and permafrost feedbacks. Nat. Geosci. **11**: 568–573.

Cory, R. M., B. C. Crump, J. A. Dobkowski, and G. W. Kling. 2013. Surface exposure to sunlight stimulates CO_2 release from permafrost soil carbon in the Arctic. Proc. Natl. Acad. Sci. USA **110**: 3429–3434.

Cory, R. M., and G. W. Kling. 2018. Interactions between sunlight and microorganisms influence dissolved organic matter degradation along the aquatic continuum. Limnol. Oceanogr. Lett. **3**: 102–116.

Cory, R. M., C. P. Ward, B. C. Crump, and G. W. Kling. 2014. Carbon cycle. Sunlight controls water column processing of carbon in arctic fresh waters. Science **345**: 925–928.

Dean, J. F., J. R. van Hal, A. J. Dolman, R. Aerts, and J. T. Weedon. 2018. Filtration artefacts in bacterial community composition can affect the outcome of dissolved organic matter biolability assays. Biogeosciences **15**: 7141–7154.

Drake, T. W., K. P. Wickland, R. G. Spencer, D. M. McKnight, and R. G. Striegl. 2015. Ancient low-molecular-weight organic acids in permafrost fuel rapid carbon dioxide production upon thaw. Proc. Natl. Acad. Sci. USA **112**: 13946–13,951.

Elder, C. D., and others. 2018. Greenhouse gas emissions from diverse Arctic Alaskan lakes are dominated by young carbon. Nat. Clim. Chang. **8**: 166–171.

Fellman, J. B., E. Hood, and R. G. M. Spencer. 2010. Fluorescence spectroscopy opens newwindows into dissolved organic matter dynamics in freshwater ecosystems: A review. Limnol. Oceanogr. **55**: 2452–2462.

Forrest, A. L., B. E. Laval, R. Pieters, and D. S. S. Lim. 2008. Convectively driven transport in temperate lakes. Limnol. Oceanogr. **53**: 2321–2332.

Fortier, D., and M. Allard. 2004. Late Holocene syngenetic ice-wedge polygons development, Bylot Island. Canadian Arctic Archipelagol. Can. J. Earth Sci. **41**: 997–1012.

Gao, X., C. Adam Schlosser, A. Sokolov, K. W. Anthony, Q. Zhuang, and D. Kicklighter. 2013. Permafrost degradation and methane: Low risk of biogeochemical climate-warming feedback. Environ. Res. Lett. **8**.

Gibson, J. A. E., W. F. Vincent, and R. Pienitz. 2001. Hydrologic control and diurnal photobleaching of CDOM in a subarctic lake. Arch. Hydrobiol. **152**: 143–159.

Groeneveld, M., L. Tranvik, S. Natchimuthu, and B. Koehler. 2016. Photochemical mineralisation in a boreal brown water lake: Considerable temporal variability and minor contribution to carbon dioxide production. Biogeosciences **13**: 3931–3943.

Grosse, G., B. Jones, and C. Arp. 2013. Thermokarst lakes, drainage, and drained basins, p. 325–353. *In* J. F. Shroder, R. Giardino, and J. Harbor [eds.], Treatise on geomorphology, Vol 8, Glacial and periglacial geomorphology. San Diego, CA: Academic Press.

Guillemette, F., and P. A. del Giorgio. 2012. Simultaneous consumption and production of fluorescent dissolved organic matter by lake bacterioplankton. Environ. Microbiol. **14**: 1432–1443.

Hansen, A. M., T. E. C. Kraus, B. A. Pellerin, J. A. Fleck, B. D. Downing, and B. A. Bergamaschi. 2016. Optical properties of dissolved organic matter (DOM): Effects of biological and photolytic degradation. Limnol. Oceanogr. **61**: 1015–1032.

Hugelius, G., and others. 2014. Estimated stocks of circumpolar permafrost carbon with quantified uncertainty ranges and identified data gaps. Biogeosciences **11**: 6573–6593.

Huguet, A., L. Vacher, S. Relexans, S. Saubusse, J. M. Froidefond, and E. Parlanti. 2009. Properties of fluorescent dissolved organic matter in the Gironde estuary. Org. Geochem. **40**: 706–719.

Knoblauch, C., C. Beer, S. Liebner, M. N. Grigoriev, and E.-M. Pfeiffer. 2018. Methane production as key to the greenhouse gas budget of thawing permafrost. Nat. Clim. Chang. **8**: 309–312.

Koehler, B., T. Landelius, G. A. Weyhenmeyer, N. Machida, and L. J. Tranvik. 2014. Sunlight-induced carbon dioxide emissions from inland waters. Global Biogeochemical Cycles **28**: 696–711.

Kortelainen, P., and others. 2006. Sediment respiration and lake trophic state are important predictors of large CO_2 evasion from small boreal lakes. Global Change Biol. **12**: 1554–1567.

Kuhry, P., and others. 2020. Lability classification of soil organic matter in the northern permafrost region. Biogeosciences **17**: 361–379.

Lapierre, J. F., and P. A. del Giorgio. 2014. Partial coupling and differential regulation of biologically and photochemically labile dissolved organic carbon across boreal aquatic networks. Biogeosciences **11**: 5969–5985.

Lara, M. J., and others. 2015. Polygonal tundra geomorphological change in response to warming alters future CO_2 and CH_4 flux on the Barrow Peninsula. Glob Chang Biol **21**: 1634–1651.

Laurion, I., P. Massicotte, F. Mazoyer, K. Negandhi, and N. Mladenov. 2020. Dissolved organic matter properties and

associated light and temperature conditions in degradation experiments with water from tundra ponds on Bylot Island, Nunavut, Canada, v. 1.0 (2010–2010). Nordicana: D56. doi: 10.5885/45618CE-5D1A86D1850841CD

Laurion, I., and N. Mladenov. 2013. Dissolved organic matter photolysis in Canadian arctic thaw ponds. Environ. Res. Lett. **8**: 035026.

Laurion, I., and others. 2010. Variability in greenhouse gas emissions from permafrost thaw ponds. Limnol. Oceanogr. **55**: 115–133.

Lennon, J. T., S. K. Hamilton, M. E. Muscarella, A. S. Grandy, K. Wickings, and S. E. Jones. 2013. A source of terrestrial organic carbon to investigate the browning of aquatic ecosystems. PLoS One **8**: e75771.

Liljedahl, A. K., and others. 2016. Pan-Arctic ice-wedge degradation in warming permafrost and its influence on tundra hydrology. Nat. Geosci. **9**: 312–318.

Lindell, M. J., W. Granéli, and L. J. Tranvik. 1995. Enhanced bacterial growth in response to photochemical transformation of dissolved organic matter. Limnol. Oceanogr. **40**: 195–199.

Loiselle, S. A., and others. 2009. The optical characterization of chromophoric dissolved organic matter using wavelength distribution of absorption spectral slopes. Limnol. Oceanogr. **54**: 590–597.

Mann, P. J., and others. 2012. Controls on the composition and lability of dissolved organic matter in Siberia's Kolyma River basin. J. Geophys. Res. Biogeosci.: 117.

Mann, P. J., and others. 2015. Utilization of ancient permafrost carbon in headwaters of Arctic fluvial networks. Nat. Commun. **6**: 7856.

Martin, A. F., T. C. Lantz, and E. R. Humphreys. 2017. Ice wedge degradation and CO_2 and CH_4 emissions in the Tuktoyaktuk Coastlands, Northwest Territories. Arctic Sci. **4**: 130–145.

McGuire, A. D., and others. 2018. Dependence of the evolution of carbon dynamics in the northern permafrost region on the trajectory of climate change. Proc Natl Acad Sci USA **115**: 3882–3887.

Miller, W. L., and M. A. Moran. 1997. Interaction of photochemical and microbial processes in the degradation of refractory dissolved organic matter from a coastal marine environment. Limnol. Oceanogr. **42**: 1317–1324.

Murphy, K. R., C. A. Stedmon, D. Graeber, and R. Bro. 2013. Fluorescence spectroscopy and multi-way techniques. PARAFAC. Anal. Methods **5**.

Murphy, K. R., C. A. Stedmon, T. D. Waite, and G. M. Ruiz. 2008. Distinguishing between terrestrial and autochthonous organic matter sources in marine environments using fluorescence spectroscopy. Mar. Chem. **108**: 40–58.

Negandhi, K., I. Laurion, and C. Lovejoy. 2014. Bacterial communities and greenhouse gas emissions of shallow ponds in the High Arctic. Polar Biol. **37**: 1669–1683.

Negandhi, K., I. Laurion, and C. Lovejoy. 2016. Temperature effects on net greenhouse gas production and bacterial communities in arctic thaw ponds. FEMS Microbiol. Ecol. **92**.

Obernosterer, I., and R. Benner. 2004. Competition between biological and photochemical processes in the mineralization of dissolved organic carbon. Limnol. Oceanogr. **49**: 117–124.

O'Reilly, C. M., and others. 2015. Rapid and highly variable warming of lake surface waters around the globe. Geophys. Res. Lett. **42**: 10773–10781.

Osburn, C. L., N. J. Anderson, M. J. Leng, C. D. Barry, and E. J. Whiteford. 2019. Stable isotopes reveal independent carbon pools across an Arctic hydro-climatic gradient: Implications for the fate of carbon in warmer and drier conditions. Limnol. Oceanogr. Lett. **4**: 205–213.

Poulin, B. A., J. N. Ryan, and G. R. Aiken. 2014. Effects of iron on optical properties of dissolved organic matter. Environ. Sci. Technol. **48**: 10098–10106.

Rantakari, M., and P. Kortelainen. 2005. Interannual variation and climatic regulation of the CO_2 emission from large boreal lakes. Glob. Chang. Biol. **11**: 1368–1380.

Roth, V.-N., and others. 2019. Persistence of dissolved organic matter explained by molecular changes during its passage through soil. Nat. Geosci. **12**: 755–761.

Schuur, E. A., and others. 2015. Climate change and the permafrost carbon feedback. Nature **520**: 171–179.

Shirokova, L. S., and others. 2019. Humic surface waters of frozen peat bogs (permafrost zone) are highly resistant to bio- and photodegradation. Biogeosciences **16**: 2511–2526.

Stedmon, C. A., and R. Bro. 2008. Characterizing dissolved organic matter fluorescence with parallel factor analysis: A tutorial. Limnol. Oceanogr. Methods **6**: 572–579.

Strome, D. J., and M. C. Miller. 1978. Photolytic changes in dissolved humic substances. Verh. Internat. Verein. Limnol. **20**: 1248–1254.

Stubbins, A., and others. 2017. Low photolability of yedoma permafrost dissolved organic carbon. J. Geophys. Res. Biogeosci. **122**: 200–211.

Suhett, A. L., A. M. Amado, A. Enrich-Prast, F. D. A. Esteves, and V. F. Farjalla. 2007. Seasonal changes of dissolved organic carbon photo-oxidation rates in a tropical humic lagoon: The role of rainfall as a major regulator. Can. J. Fish. Aquat. Sci. **64**: 1266–1272.

Surdu, C. M., C. R. Duguay, and D. Fernández Prieto. 2016. Evidence of recent changes in the ice regime of lakes in the Canadian High Arctic from spaceborne satellite observations. The Cryosphere **10**: 941–960.

Tank, S. E., J. E. Vonk, M. A. Walvoord, J. W. McClelland, I. Laurion, and B. W. Abbott. 2020. Landscape matters: Predicting the biogeochemical effects of permafrost thaw on aquatic networks with a state factor approach. Permafrost Periglac. **31**: 358–370.

Turetsky, M. R., and others. 2020. Carbon release through abrupt permafrost thaw. Nat. Geosci. **13**: 138–143.

Vachon, D., J.-F. Lapierre, and P. A. del Giorgio. 2016. Seasonality of photochemical dissolved organic carbon mineralization and its relative contribution to pelagic CO_2 production in northern lakes. J. Geophys. Res. Biogeosci. **121**: 864–878.

Vähätalo, A. V., K. Salonen, U. Münster, M. Järvinen, and R. G. Wetzel. 2003. Photochemical transformation of allochthonous organic matter provides bioavailable nutrients in a humic lake. Arch. Hydrobiol. **156**: 287–314.

von Wachenfeldt, E., and L. J. Tranvik. 2008. Sedimentation in boreal lakes - the role of flocculation of allochthonousdissolved organic matter in the water column. Ecosystems **11**: 803–814.

Vonk, J. E., and others. 2013. High biolability of ancient permafrost carbon upon thaw. Geophys. Res. Lett. **40**: 2689–2693.

Vonk, J. E., and others. 2015. Biodegradability of dissolved organic carbon in permafrost soils and aquatic systems: A meta-analysis. Biogeosciences **12**: 6915–6930.

Ward, C. P., S. G. Nalven, B. C. Crump, G. W. Kling, and R. M. Cory. 2017. Photochemical alteration of organic carbon draining permafrost soils shifts microbial metabolic pathways and stimulates respiration. Nat. Comm. **8**: 772.

Wauthy, M., and others. 2018. Increasing dominance of terrigenous organic matter in circumpolar freshwaters due to permafrost thaw. Limnol. Oceanogr. Lett. **3**: 186–198.

Wen, H., and others. 2020. Temperature controls production but hydrology regulates export of dissolved organic carbon at the catchment scale. Hydrol. Earth Syst. Sci. **24**: 945–966.

Wetzel, R. G., P. G. Hatcher, and T. S. Bianchi. 1995. Natural photolysis by ultraviolet irradiance of recalcitrant dissolved organic matter to simple substrates for rapidbacterial metabolism. Limnol. Oceanogr. **40**: 1369–1380.

Wickland, K. P., M. P. Waldrop, G. R. Aiken, J. C. Koch, M. T. Jorgenson, and R. G. Striegl. 2018. Dissolved organic carbon and nitrogen release from boreal Holocene permafrost and seasonally frozen soils of Alaska. Environ. Res. Lett **13**: 065011.

Williams, C. J., P. C. Frost, and M. A. Xenopoulos. 2013. Beyond best management practices:Pelagic biogeochemical dynamics in urban stormwater ponds. Ecol. Appl. **23**: 1384–1395.

Williamson, C. E., and others. 2014. Solar ultraviolet radiation in a changing climate. Nat. Clim. Chang. **4**: 434–441.

Wrona, F. J., and others. 2016. Transitions in Arctic ecosystems: Ecological implications of a changing hydrological regime. J. Geophys. Res. Biogeosci **121**: 650–674.

Acknowledgments

Conflict of interest

None declared.